

TESS Observations of the Hot Jupiter Exoplanet XO-6b: No Evidence of Transit Timing Variations

ANDREW RIDDEN-HARPER ¹, JAKE D. TURNER ¹ AND RAY JAYAWARDHANA²

¹*Department of Astronomy and Carl Sagan Institute, Cornell University, Ithaca, New York 14853, USA*

²*Department of Astronomy, Cornell University, Ithaca, New York 14853, USA*

(Accepted September, 19, 2020)

Submitted to AJ

ABSTRACT

From previous ground-based observations, the hot Jupiter exoplanet XO-6b was reported to exhibit apparently periodic transit timing variations (TTVs), with a semi-amplitude of 14 minutes and a period of about 450 days. These variations were interpreted as being due to a resonant perturbation between XO-6b and a hitherto unknown low-mass planet orbiting the same star. To understand this enigmatic planetary system better, we analysed three sectors of data, spanning over seven months, from the Transiting Exoplanet Survey Satellite (TESS), which produces high-quality light curves that are well suited to characterizing exoplanets and searching for TTVs. Here we present an updated orbital period of 3.7649893 ± 0.0000037 days and a transit epoch of 2456652.7157 ± 0.0022 BJD_{TDB}. The planetary parameters we report, while consistent with their discovery values, have greatly improved precision. Notably, we find no evidence for TTVs: we can rule out TTVs $\gtrsim 2.5$ minutes at the 3σ level. Therefore, the TESS data have sufficient precision and time baseline to reveal readily the previously reported TTVs of approximately 10 minutes. Our findings highlight TESS's capabilities for robust follow-up, and confirm that TTVs are rarely seen in hot Jupiters, unlike is the case with small planets.

Keywords: planets and satellites: dynamical evolution and stability — planets and satellites: gaseous planets — planetstar interactions — planets and satellites: individual (XO-6b) — methods: observational — techniques: photometric

1. INTRODUCTION

Gravitational interactions between bodies in a planetary system can cause a transiting exoplanet's time of transit to vary. Analysis of such transit timing variations (TTVs) can reveal important dynamical insights into a planetary system. About 130 small planets were found to exhibit TTVs from *Kepler* data (Mazeh et al. 2013). However, TTVs have only been observed in a handful of hot Jupiters. For example, a variation in the transit time and impact parameter of Kepler-13Ab has revealed evidence for spin-orbit precession caused

by its host star's rapidly rotating quadrupole moment (e.g., Masuda 2015; Herman et al. 2018; Szabó et al. 2020), allowing the stellar surface to be mapped (Szabó et al. 2014). Becker et al. (2015) found that WASP-47b exhibits sinusoidal TTVs caused by two smaller short-period planets in the same system. WASP-12b also exhibits TTVs, presumably resulting from orbital decay or apsidal precession (Maciejewski et al. 2016; Patra et al. 2017; Maciejewski et al. 2018); recently Yee et al. (2020) offered new evidence that favors tidally-induced orbital decay as the explanation.

The Transiting Exoplanet Survey Satellite (TESS) (Ricker et al. 2014) produces high-quality data that are well suited to searching for TTVs (e.g. Hadden et al. 2019; Pearson 2019). Using TESS data, Bouma et al. (2019) found that the transits of WASP-4b occurred about 82 seconds earlier than expected, and determined that its 1.3-day orbital period is decreasing at a rate

Corresponding author: Andrew Ridden-Harper
arr224@cornell.edu

Corresponding author: Jake D. Turner
astrojaketurner@gmail.com, jaketurner@cornell.edu

of about -12.6 ± 1.2 ms per year. Southworth et al. (2019) confirmed the presence of TTVs, but revised the orbital period decay rate to -9.2 ± 1.1 ms per year. More recently, a homogeneous analysis of 124 transits of WASP-4b, observed with several different telescopes, found that its rate of change in orbital period is about half that found in previous studies (Baluev et al. 2019, 2020). Finally, Bouma et al. (2020) found that its orbital period changes by -8.64 ms per year. While it has been suggested that these TTVs may arise from orbital decay or apsidal precession (Southworth et al. 2019), recent findings indicate that they are due to the system accelerating towards the Sun at a rate of -0.0422 ms^{-1} day^{-1} (Bouma et al. 2020).

Here we focus on the hot Jupiter XO-6b, with a mass and radius of $1.9 R_{Jup}$ and $2.07 M_{Jup}$, respectively. It orbits a fast-rotating ($v \sin i = 48$ kms^{-1}), bright ($V = 10.25$ mag), hot ($T_{eff} = 6720$ K) star and has an orbital period of 3.8 days (Crouzet et al. 2017). To characterize XO-6b better, Garai et al. (2020) observed its transits with telescopes at the Astronomical Institute of the Slovak Academy of Sciences and downloaded transit light curves from the Exoplanet Transit Database (ETD)¹ (Poddaný et al. 2010). From these data, they reported that it exhibited intriguing periodic TTVs with a semi-amplitude of 14 minutes and period of about 450 days. By fitting these transit timing variations with the publicly available TTV analysis package, OCFit² (Gajdoš & Parimucha 2019), they determined the two most plausible explanations to be 1) light-time effects (LiTE) due to a third unknown stellar-mass object in the XO-6 system, or 2) resonant perturbations between XO-6b and an unknown low-mass planet in the system. However, they found no evidence for a stellar mass object in radial velocity (RV) follow-up, and simultaneous fits to their transit timing and RV measurements did not yield a consistent solution; so they favor the second interpretation. If the latter interpretation were correct, the XO-6b system would resemble the recently discovered TOI-216 system which contains a pair of warm, large exoplanets that exhibit planet-planet interactions (Dawson et al. 2019; Dawson 2020).

Motivated by the intriguing TTVs of XO-6b reported by Garai et al. (2020), we investigated this system further by analysing its TESS light curves. Our paper is structured as follows. Section 2 describes our data reduction method. Section 3 shows our analysis and Sec-

tion 4 presents and discusses our results. Finally, Section 5 offers our conclusions.

2. OBSERVATIONS

XO-6b was observed by TESS in Sector 19 (November 27, 2019 to December 24, 2019), Sector 20 (December 24, 2019 to January 21, 2020) and Sector 26 (June 8, 2020 to July 4, 2020). These observations were processed by the Science Processing Operations Center (SPOC) pipeline, which produces light curves corrected for systematics and searches for transiting planets (Jenkins et al. 2016). All of the data products produced by SPOC are publicly available from the Mikulski Archive for Space Telescopes (MAST)³. We downloaded all of the data products for XO-6b, including the light curve (LC) files, data validation timeseries (DVT) files, and target pixel files (TPFs). The Presearch Data Conditioning (PDC) component of the SPOC pipeline corrects the light curves for pointing or focus related instrumental signatures, discontinuities resulting from radiation events in the CCD detectors, outliers, and flux contamination (Jenkins et al. 2016). The light curve resulting from the PDC corrections is recorded as the PDCSAP_FLUX, and was one of the data products considered in our analysis. The PDCSAP_FLUX is further processed by using a running median filter to remove any long-period systematics before the SPOC pipeline searches for transits⁴. The length of the running median filter that was used is recorded in the file headers and in the case of the XO-6b data was 14.8, 15.2, and 15.0 hours in Sectors 19, 20 and 26, respectively. These light curves are recorded in the DVT file as LC_INIT and were also considered in our analysis.

For comparison, we also considered light curves that we produced from the TPFs using aperture photometry. To do this, we followed the documentation⁵ accompanying the `exoplanet` package (Foreman-Mackey et al. 2020). We selected the optimal aperture that minimized the windowed scatter and detrended the resulting light curve with the pixel-level deconvolution (PLD) method used by the `Everest` package (Luger et al. 2016).

Of the three light curve detrendings that we considered, the DVT light curve had the least scatter, with a standard deviation on the out-of-transit baseline of 1.08 ppt, which was 3% and 13% lower than that of our light curves from the TPFs and the PDCSAP_FLUX, respectively. Therefore, we focused on the DVT light curves in

¹ <http://var2.astro.cz/ETD/>

² <https://github.com/pavolgaj/OCFit>

³ <https://archive.stsci.edu/>

⁴ <https://exoplanetarchive.ipac.caltech.edu/docs/DVSummaryPageCompanion.html>

⁵ <https://exoplanet.readthedocs.io/en/v0.1.6/tutorials/tess/>

our analysis. Nonetheless, we also analysed the transit timings of the other light curves and found them to be practically identical to what was derived from the DVT light curves (see Appendix A; Fig. 4). The raw light curve produced by the SPOC and detrended DVT light curve used in this analysis are shown in Figure 1.

3. DATA ANALYSIS

To find the best-fit to the TESS transits we use the EXOplanet MOdeling Package (EXOMOP; Pearson et al. 2014; Turner et al. 2016, 2017)⁶, which generates a model transit using the analytic equations of Mandel & Agol (2002). EXOMOP uses a Differential Evolution Markov Chain Monte Carlo (DE-MCMC; Braak 2006; Eastman et al. 2013) analysis to model the data and incorporates three different red noise methods (time-averaging, Pont et al. 2006; residual permutation, Southworth 2008; wavelet, Carter & Winn 2009) to assess and account for red noise in the light curve. A thorough description of EXOMOP can be found in Pearson et al. (2014) and Turner et al. (2016).

We model each transit event in the TESS data (lower panel of Figure 1) independently. Each transit is modeled with 20 chains and 20^6 links for the DE-MCMC model and we use the Gelman-Rubin statistic (Gelman & Rubin 1992) to ensure chain convergence (Ford 2006). For each transit, the mid-transit time (T_c), planet-to-star radius (R_p/R_*), scaled semi-major axis (a/R_*), and inclination (i) are set as free parameters. The eccentricity, argument of periastron, period (P_{orb}), and linear and quadratic limb darkening coefficients are fixed during the analysis. The linear and quadratic limb darkening coefficients are taken from Claret (2017) and are equal to 0.3158 and 0.2206, respectively. The light curve parameters derived for each individual transit can be found in Table 2 and the individual modeled light curves can be found in Figures 5–7 in Appendix B. All parameters for each transit event are consistent within 1σ of every other transit.

To obtain the final fitted parameters, the light curve of XO-6b was phase-folded at each individual derived mid-transit time and modeled with EXOMOP. The phase-folded light curve and model fit can be found in Figure 2. We use the light curve model results combined with literature values to calculate the planetary radius (R_b), mass (M_b ; Winn 2010), density (ρ_b), surface gravity ($\log g_b$; Southworth et al. 2007), equilibrium temperature (T_{eq}), Safronov number (Θ ; Safronov 1972; Southworth 2010), orbital distance (a), inclination, and stellar density (ρ_{*a} ;

Table 1. Physical properties of XO-6b derived from the light curve modeling of the TESS data

| Parameter | units | value | 1σ uncertainty |
|-------------|--------------------|--------------|-----------------------|
| R_p/R_* | | 0.11494 | 0.00029 |
| a/R_* | | 8.383 | 0.074 |
| Inclination | $^\circ$ | 85.235 | 0.087 |
| Duration | mins | 179.94 | 0.11 |
| b | | 0.696 | 0.014 |
| R_b | R_{Jup} | 2.08 | 0.18 |
| M_b | M_{Jup} | 2.01 | 0.71 |
| ρ_b | g cm^{-3} | 0.28 | 0.12 |
| $\log g_b$ | cgs | 3.31 | 0.19 |
| ρ_{*a} | g cm^{-3} | 0.786 | 0.09642 |
| T_{eq} | K | 1641 | 24 |
| Θ | | 0.093 | 0.035 |
| a | au | 0.0725 | 0.0063 |
| Period | day | 3.7649893 | 0.0000037 |
| $T_c(0)$ | BJD_{TDB} | 2456652.7157 | 0.0022 |

Seager & Mallén-Ornelas 2003). The period (P_{orb}) and transit ephemeris ($T_C[0]$) are derived using the mid-transit times from each TESS transit event (Table 2). Our derived planet properties and transit ephemeris for XO-6b are shown in Table 1. All the planetary parameters are consistent with their discovery values (Crouzet et al. 2017) but their precision is greatly improved.

Transit timing variations are conveniently studied in terms of O–C, where O is the observed transit time and C is the corresponding calculated transit time. We calculated C with the linear ephemeris formula

$$T_E = T_0 + P_{orb} \times E \quad (1)$$

where T_0 is the reference transit time, P_{orb} is the orbital period, E is the transit epoch, and T_E is the calculated transit time at epoch E .

For research requiring accurate timing, it is important to consider the clock accuracy and the time standard that are used because ambiguity between different standards can produce spurious timing effects that could be mistaken for TTVs or bias eccentricity measurements (Eastman et al. 2010). The time stamps of the data products produced by the TESS SPOC pipeline are TESS Julian Dates (TESS JD = JD–2457000.0) in the Barycentric Dynamical Time standard, BJD_{TDB} ⁷, which is usually the most accurate time standard to use as it accounts for many different timing corrections, including leap seconds (e.g., Eastman et al. 2010). This

⁶ EXOMOPv7.0; <https://github.com/astrojake/EXOMOP>

⁷ https://archive.stsci.edu/files/live/sites/mast/files/home/missions-and-data/active-missions/tess/_documents/TESS_Instrument_Handbook.v0.1.pdf

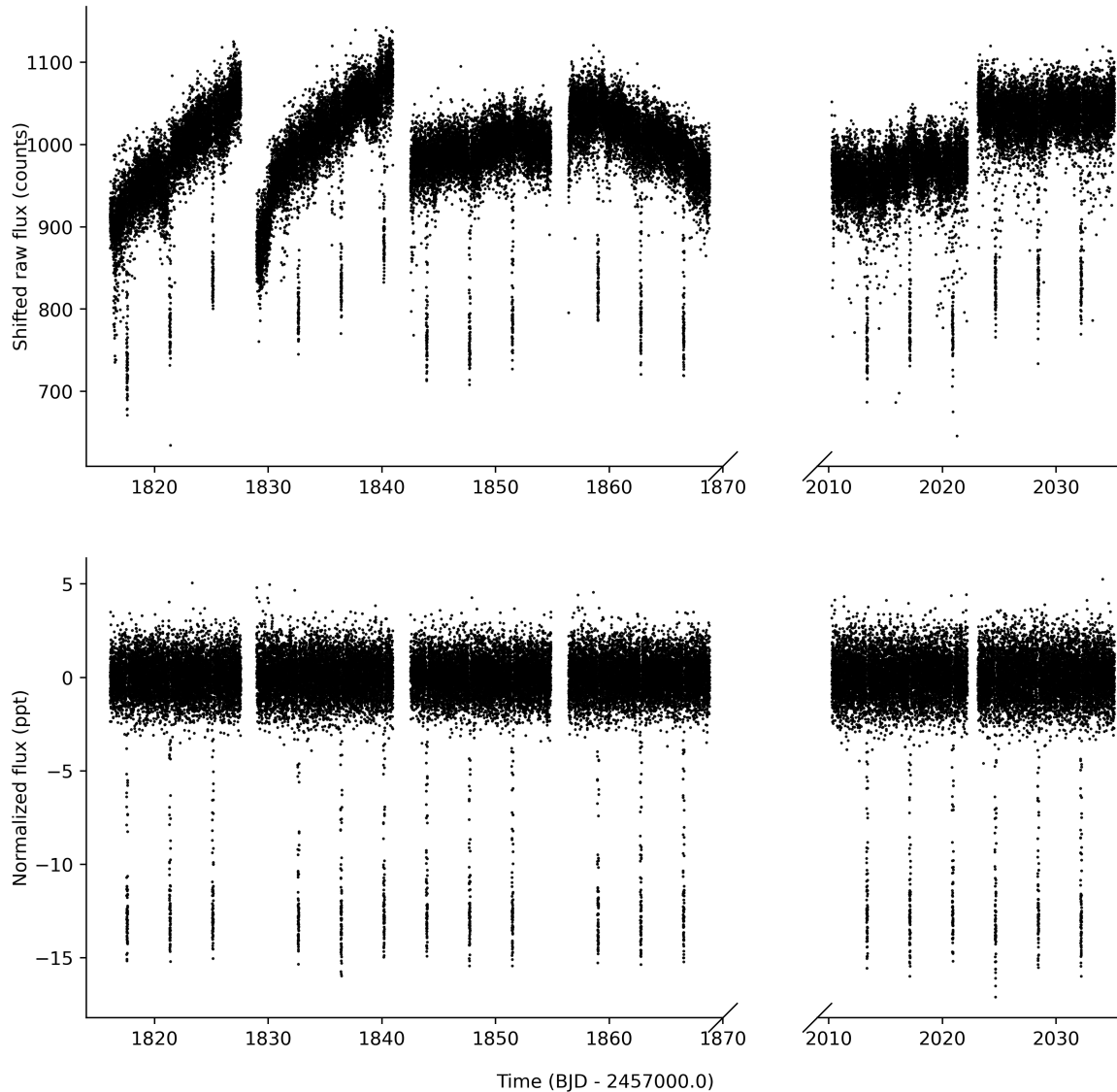


Figure 1. TESS light curve of XO-6b in Sectors 19, 20 and 26. Top: Raw simple aperture photometry light curves, shifted vertically for clarity. Bottom: Detrended Data Validation Timeseries (DVT).

is achieved with a series of time conversions outlined as follows. Time stamps are first recorded by the 1 Hz spacecraft clock aboard TESS. While the frequency of this clock drifts due to thermal and aging effects, it is correlated with Coordinated Universal Time (UTC) by the Mission Operations Center at every contact, which occurs approximately every three days. The Payload Operations Center then converts the spacecraft clock counts into TESS Julian Day before passing it to the SPOC for a final conversion into BJD_{TDB} ⁸. This final conversion is implemented with the same algorithm that

was used for *Kepler*, and works by using the Navigation and Ancillary Interface (NAIF) SPICE kernel trajectory file⁹ to calculate the projected distance to the solar system barycenter and the resulting timing corrections for each star in the TESS field of view (Jenkins, J., private communication). By analysing contemporaneous TESS and ground-based observations of several binary star systems, von Essen et al. (2020) showed that the TESS BJD_{TDB} times are correct to an absolute precision of <6 seconds.

Figure 3 shows the O–C values we derived from the TESS observations, along with the O–C values and

⁸ https://archive.stsci.edu/files/live/sites/mast/files/home/missions-and-data/active-missions/tess/_documents/TESS_Instrument_Handbook_v0.1.pdf

⁹ <https://naif.jpl.nasa.gov/naif/index.html>

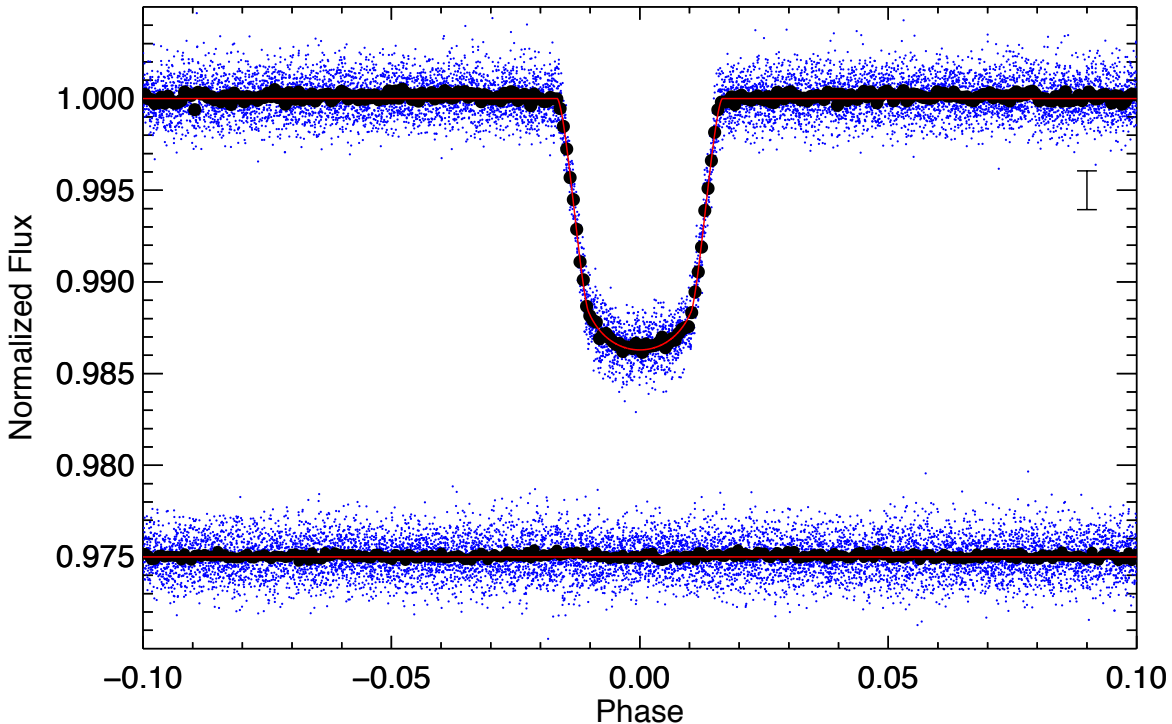


Figure 2. Phased folded light curve of XO-6b from TESS. The unbinned and binned data are shown in blue and black, respectively. The best-fitting model obtained from the EXOplanet MODELing Package (EXOMOP) is shown as a solid red line. The residuals (light curve - model) are shown below the light curve.

best fit light-time effect (LiTE) model from Garai et al. (2020). To compare our transit times to this model, we used the publicly available OCFit package¹⁰ (Gajdoš & Parimucha 2019) to reproduce it using their fitted parameters shown in Table 3 in Appendix C. While this model is a good fit to their reported TTVs, they did not observe radial velocities consistent with the XO-6 star-planet system having a stellar mass companion capable of inducing these light-time effects. Therefore, they favor the interpretation that these TTVs are caused by resonant perturbations between XO-6b and another unknown low-mass planet in the system, although they do not quantify the mass of their suggested perturbing planet.

4. RESULTS AND DISCUSSION

Our analysis of the TESS data of XO-6b yielded an updated orbital period and a transit epoch of 3.7649893 ± 0.0000037 days and 2456652.7157 ± 0.0022 BJD_{TDB} , respectively.

Notably, we did not find any evidence of transit timing variations in the case of XO-6b, despite the TESS data having sufficient precision and time baseline to clearly reveal the TTVs reported by Garai et al. (2020). Specifically, the 3σ upper-limit on TTVs allowed by the TESS

observations is 2.5 minutes, while their LiTE model predicts TTVs of 12-14 minutes in Sectors 19 and 20 and 5-9 minutes in Sector 26. Therefore, the TESS data rule out their LiTE model by $14\text{-}16\sigma$ in Sectors 19 and 20 and $6\text{-}11\sigma$ in Sector 26. While the cause of this discrepancy is not clear, here we discuss some possible explanations.

The analysis of Garai et al. (2020) utilized 15 transits, of which 8 were observed by the authors themselves with telescopes at the Astronomical Institute of the Slovak Academy of Sciences and 7 were adopted from the ETD after having been observed by others. While the data obtained from the ETD do not exhibit stronger TTVs than their own observations (see Figure 8 in Appendix D) and they only used data from the ETD that had clearly indicated timing epochs (either JD or HJD) and good quality, it is still possible these data points introduced unaccounted for uncertainties that contributed to the discrepancy. We used the `astropy.time`¹¹ package to calculate the barycentric correction for the data used by Garai et al. (2020) and found that it ranges from -5 to $+5$ minutes, with a mean value of $+0.8$ minutes (see Figure 8 in Appendix D). Therefore, while a few of the smaller TTVs they reported could be related to

¹⁰ <https://github.com/pavolgaj/OCFit>

¹¹ <https://docs.astropy.org/en/stable/time/>

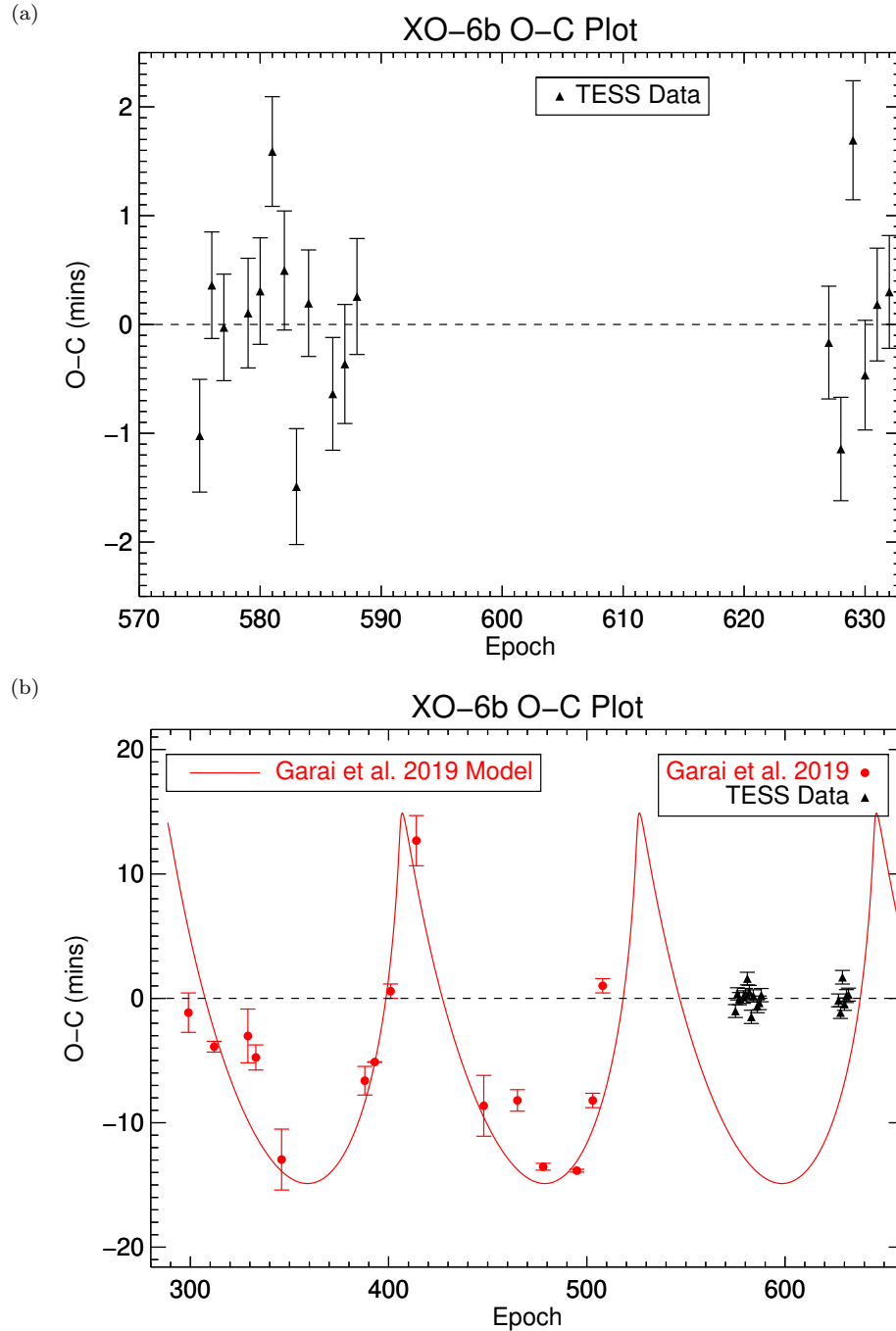


Figure 3. a.) The observation minus calculation mid-transit time (O-C) diagram derived using the TESS data (black). b.) The O-C diagram including data points from Garai et al. (2020) (red). The best-fit light-time effect (LiTE) model from Garai et al. (2020) is shown as a red line.

barycentric corrections, the larger ones must have other causes.

Garai et al. (2020) also utilized spectroscopic radial velocity (RV) observations, which showed no evidence of an additional body in the XO-6 system. Furthermore, simultaneous fits to their RV and O-C data did

not produce a consistent solution, potentially suggesting spurious effects.

Crouzet et al. (2017) found no evidence of XO-6b exhibiting TTVs, which Garai et al. (2020) attributed to the Crouzet et al. (2017) observations covering a relatively short time span, having non-optimal time sampling, and/or higher uncertainties in their O-C values.

However, the results of [Crouzet et al. \(2017\)](#) and [Garai et al. \(2020\)](#) could also be reconciled if the findings of [Garai et al. \(2020\)](#) were affected by unknown timing errors.

The presence or absence of companion planets near a hot Jupiter are indicative of how it formed ([Steffen et al. 2012](#)). The vast majority of transiting hot Jupiters are the only transiting planet in their system (e.g., [Huang et al. 2016](#)) so our interpretation that XO-6b does not have a companion is consistent with this clear trend. The trend could arise either because the systems do not contain any other planets or because they contain planets on inclined orbits that do not transit.

[Spalding & Batygin \(2016\)](#) showed that hot stars like XO-6 with $T_{eff} > 6200$ K can exert torques on their planets that increase their inclinations so that they do not transit. This effect is stronger for closer-in planets, potentially resulting in a planetary system harboring only one transiting planet.

[Batygin et al. \(2016\)](#) argue that a substantial fraction of the hot-Jupiter population formed in situ. They showed that this process would lead frequently to hot-Jupiters being accompanied by low-mass planets with periods shorter than approximately 100 days. Furthermore, they found that dynamical interactions early in the systems' lifetimes should increase the inclinations of these companions, making them unlikely to transit.

While the presence of an additional non-transiting planet in the XO-6 system would be consistent with the interpretation of [Garai et al. \(2020\)](#), [Nesvorný \(2009\)](#) showed that the TTV signal caused by inclined non-transiting companions may be more pronounced than that caused by co-planar companions. Therefore, if XO-6b does have a non-coplanar, non-transiting companion, it is reasonable to expect that it could be detected. Rigorous modelling could constrain the allowed parameter space of a potential candidate while still being consistent with XO-6b not showing any transit timing variations (e.g., [Hrudková et al. 2010](#)), but that is beyond the scope of the present study.

Alternatively, [Mustill et al. \(2015\)](#) show that if a hot Jupiter reaches its current orbit by high-eccentricity migration, any inner low-mass planets will collide with their host star or the migrating giant planet and be destroyed. The initial high eccentricity required for this process can be produced by planet-planet scattering, the Kozai effect or low-inclination secular interactions. Once the giant planet's pericenter has migrated to within a few hundredths of an AU from its host star, its orbit will be tidally circularized, resulting in a hot Jupiter with a very low eccentricity, such as XO-6b.

Given the lack of evidence for an additional non-transiting planet in the system, we consider it likely that XO-6b migrated inwards to its current orbital distance. Future observational constraints on XO-6b's atmospheric C/O ratio, which would be indicative of where a planet formed in a protoplanetary disk, could confirm such a scenario (e.g., [Öberg et al. 2011](#); [Cridland et al. 2019](#)).

5. CONCLUSION

We utilized publicly available TESS data to further characterize the hot-Jupiter XO-6b. Our analysis yielded an updated period of 3.7649893 ± 0.0000037 days and transit epoch of 2456652.7157 ± 0.0022 BJD_{TDB}. Moreover, we found no evidence of the transit timing variations reported by [Garai et al. \(2020\)](#), despite the precision and time baseline of the TESS data being sufficient to reveal them, highlighting the usefulness of TESS follow-up observations of interesting targets found with ground-based observations. The cause of the tension between our results and those of [Garai et al. \(2020\)](#) is not clear but it may be due to unknown timing errors in their ground-based data. This underscores the importance of careful absolute telescope clock calibrations and considerations of timing standards ([Eastman et al. 2010](#)), which is not only necessary for TTV analysis, but also for constraining ephemerides well enough to enable efficient scheduling of atmospheric characterization observations on high-demand telescopes like the upcoming James Webb Space Telescope and the 30-meter class telescopes ([Dragomir et al. 2020](#); [Zellem et al. 2020](#)).

ACKNOWLEDGMENTS

We thank Thomas Barclay and Jon Jenkins for assisting us to fully utilize the TESS/SPOC data products, and Ernst de Mooij for helpful discussions. We also thank the anonymous referee for their constructive suggestions. This paper includes data collected by the TESS mission, which are publicly available from the Mikulski Archive for Space Telescopes (MAST). Funding for the TESS mission is provided by the NASA Explorer Program.

This research has made use of the Extrasolar Planet Encyclopaedia, NASA's Astrophysics Data System Bibliographic Services, and the NASA Exoplanet Archive, which is operated by the California Institute of Technology, under contract with the National Aeronautics and Space Administration under the Exoplanet Exploration Program.

Facilities: TESS

Software: `astropy` (Astropy Collaboration et al. 2013), `EXOMOP` (Pearson et al. 2014; Turner et al. 2016, 2017), `OCFit` (Gajdoš & Parimucha 2019), `exoplanet` package (Foreman-Mackey et al. 2020), `Everest` package (Luger et al. 2016)

APPENDIX

A. DIFFERENCE IN MID-TRANSIT TIMES BETWEEN DIFFERENT DETRENDING MODELS

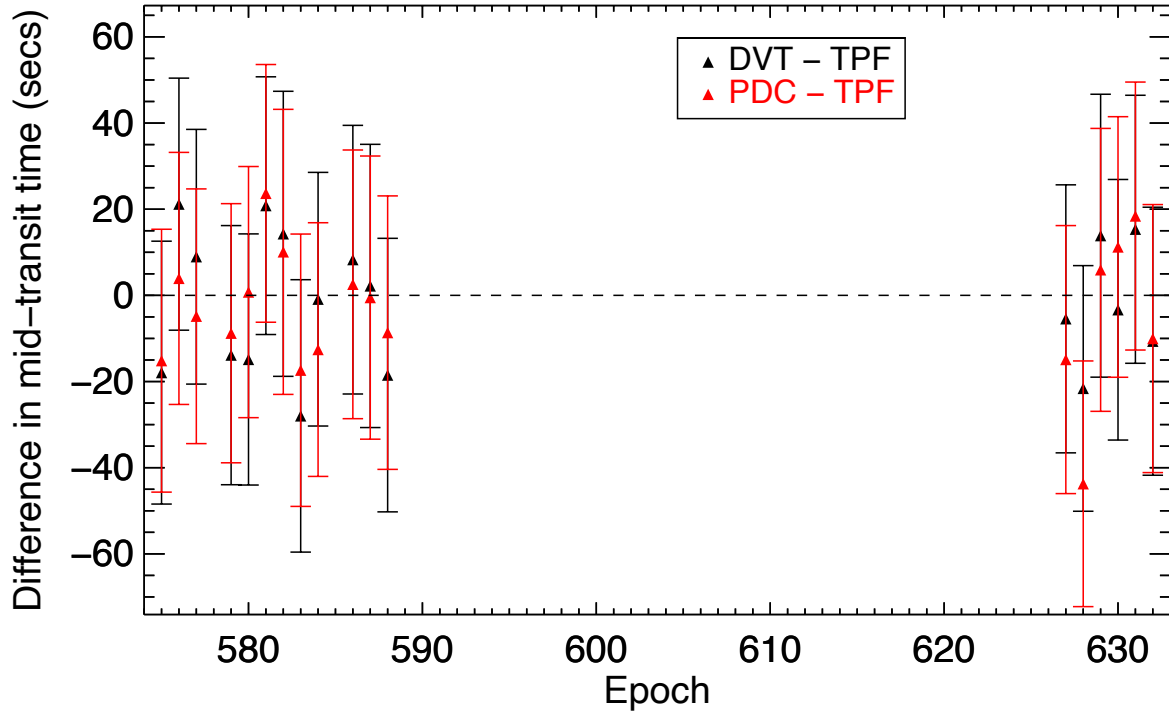


Figure 4. Differences in derived mid-transit times relative to our detrended light curve produced from the target pixel files (TPFs) for the data validation timeseries (DVT) (black) and the Presearch Data Conditioning (PDCSAP_FLUX) (red).

B. TRANSIT FITS TO INDIVIDUAL TESS TRANSIT EVENTS

Table 2. Individual TESS transit parameters for XO-6b derived using EXOMOP

| Sector 19 | | | |
|-------------------------------------|-------------------|-------------------|-------------------|
| Transit | 1 | 2 | 3 |
| T_c (BJD _{TDB} -2458810) | 7.58383±0.00036 | 11.34978±0.00033 | 15.11450±0.00030 |
| R_p/R_* | 0.1141±0.0011 | 0.1148±0.0011 | 0.1130±0.0010 |
| a/R_* | 8.73±0.36 | 8.49±0.33 | 8.91±0.27 |
| Inclination (°) | 85.62±0.39 | 85.25±0.37 | 85.83±0.32 |
| Duration (days) | 174.02±3.05 | 174.02±2.88 | 174.02±2.83 |
| Transit | 4 | 5 | 6 |
| T_c (BJD _{TDB} -2458810) | 22.64457±0.00035 | 26.40970±0.00032 | 30.17558±0.00033 |
| R_p/R_* | 0.1158±0.0011 | 0.1159±0.0014 | 0.1133±0.0012 |
| a/R_* | 8.38±0.29 | 8.64±0.37 | 8.62±0.34 |
| Inclination (°) | 85.21±0.34 | 85.44±0.43 | 85.55±0.41 |
| Duration (days) | 177.89±2.83 | 174.02±2.87 | 175.96±2.90 |
| Sector 20 | | | |
| Transit | 1 | 2 | 3 |
| T_c (BJD _{TDB} -2458810) | 33.93981±0.00035 | 37.70342±0.00030 | 41.46958±0.00032 |
| R_p/R_* | 0.1154±0.0012 | 0.11425±0.00088 | 0.11550±0.00082 |
| a/R_* | 7.95±0.27 | 8.59±0.249 | 8.13± |
| Inclination (°) | 84.75±0.35 | 85.51±0.27 | 84.96±0.24 |
| Duration (days) | 183.87±2.86 | 175.96±2.86 | 181.93±2.83 |
| Transit | 4 | 5 | 6 |
| T_c (BJD _{TDB} -2458810) | 48.99898±0.00034 | 52.76416±0.00037 | 56.52958±0.00036 |
| R_p/R_* | 0.1143±0.0012 | 0.11789±0.00099 | 0.1153±0.0011 |
| a/R_* | 8.55±0.36 | 7.58±0.23 | 8.09±0.28 |
| Inclination (°) | 85.44±0.40 | 84.23±0.30 | 84.91±0.35 |
| Duration (days) | 176.13±2.85 | 184.04±2.87 | 180.00±2.85 |
| Sector 26 | | | |
| Transit | 1 | 2 | 3 |
| T_c (BJD _{TDB} -2458810) | 203.36387±0.00036 | 207.12818±0.00033 | 210.89514±0.00038 |
| R_p/R_* | 0.1142±0.0015 | 0.1149±0.0012 | 0.1149±0.0012 |
| a/R_* | 8.55±0.43 | 8.52±0.33 | 8.29±0.35 |
| Inclination (°) | 85.50±0.52 | 85.41±0.40 | 85.10±0.41 |
| Duration (days) | 178.07±2.88 | 177.89±2.85 | 178.07±2.92 |
| Transit | 4 | 5 | 6 |
| T_c (BJD _{TDB} -2458810) | 214.65863±0.00035 | 218.42407±0.00036 | 222.18914±0.00036 |
| R_p/R_* | 0.1169±0.0011 | 0.1135±0.0010 | 0.11576±0.00097 |
| a/R_* | 8.47±0.26 | 8.66±0.26 | 8.13±0.21 |
| Inclination (°) | 85.30±0.31 | 85.57±0.30 | 84.92±0.25 |
| Duration (days) | 175.96±2.86 | 174.02±2.91 | 180.00±2.88 |

NOTE—The linear and quadratic limb darkening coefficient used in the analysis are 0.3158 and 0.2206 (Claret 2017)

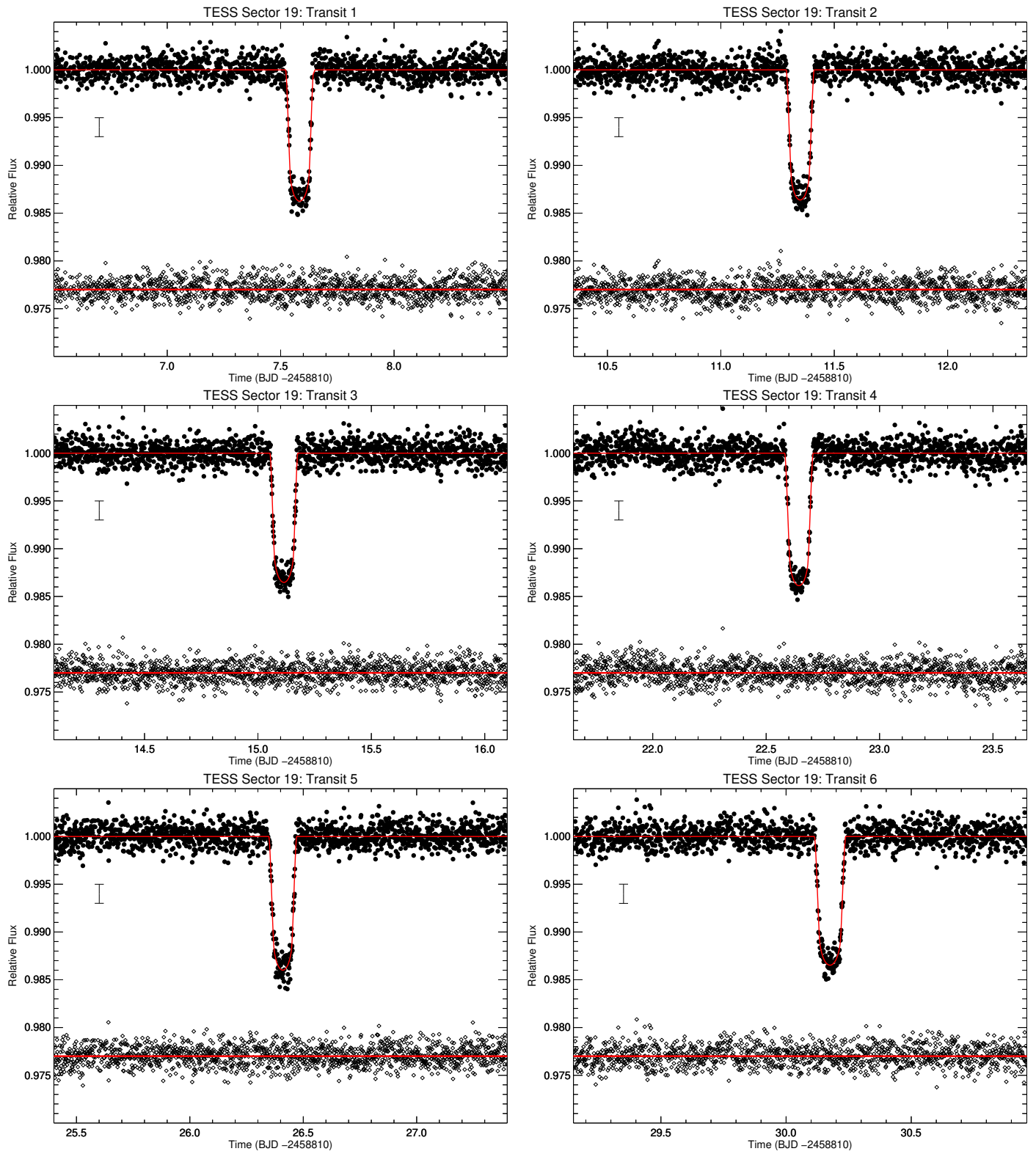


Figure 5. Individual TESS transit events from Sector 19 of XO-6b. The best-fitting model obtained from the EXOplanet Modeling Package (EXOMOP) is shown as a solid red line. The residuals (light curve - model) are shown below the light curve.

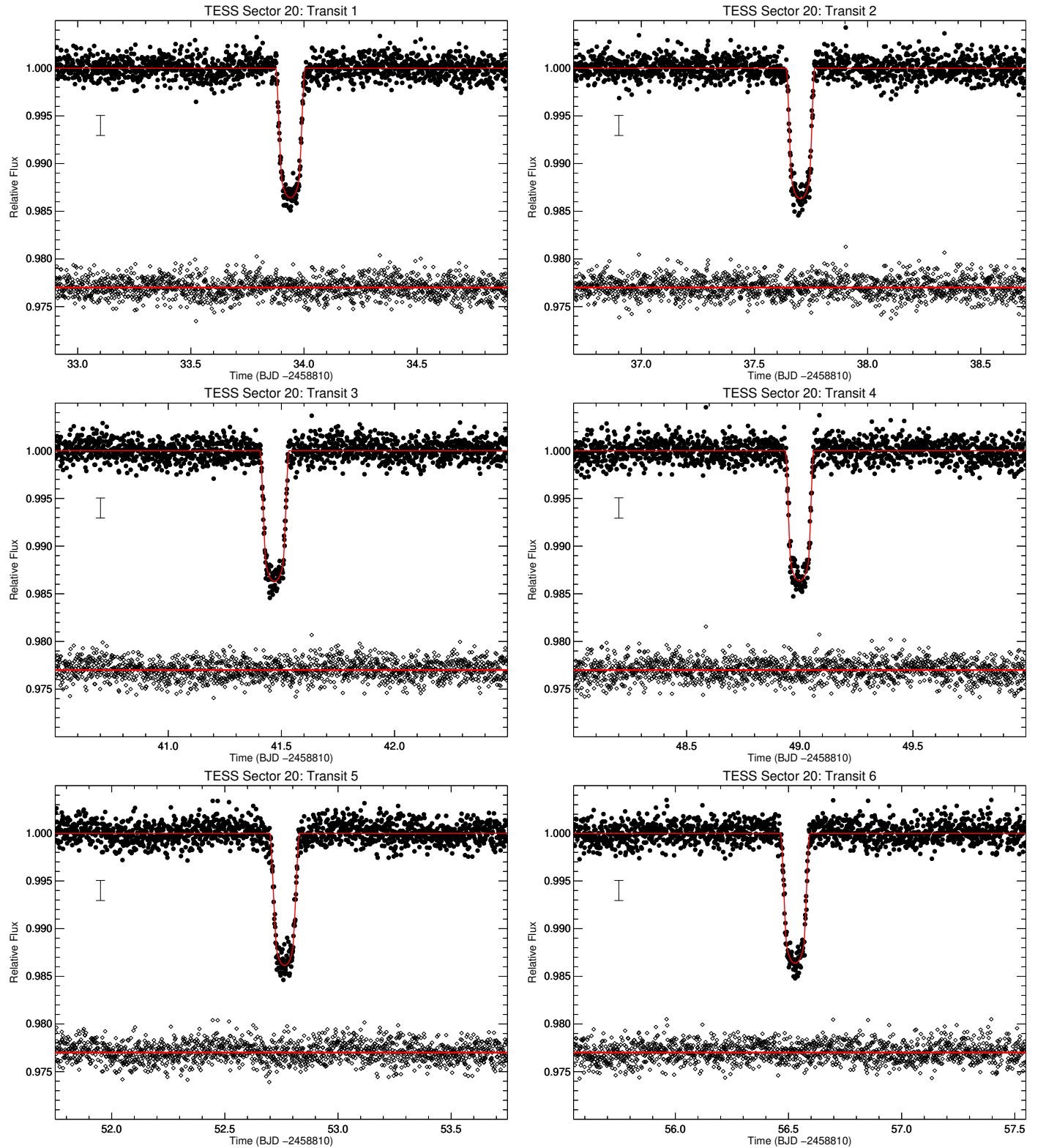


Figure 6. Individual TESS transit events from Sector 20 of XO-6b. The best-fitting model obtained from the EXOplanet Modeling Package (EXOMOP) is shown as a solid red line. The residuals (light curve - model) are shown below the light curve.

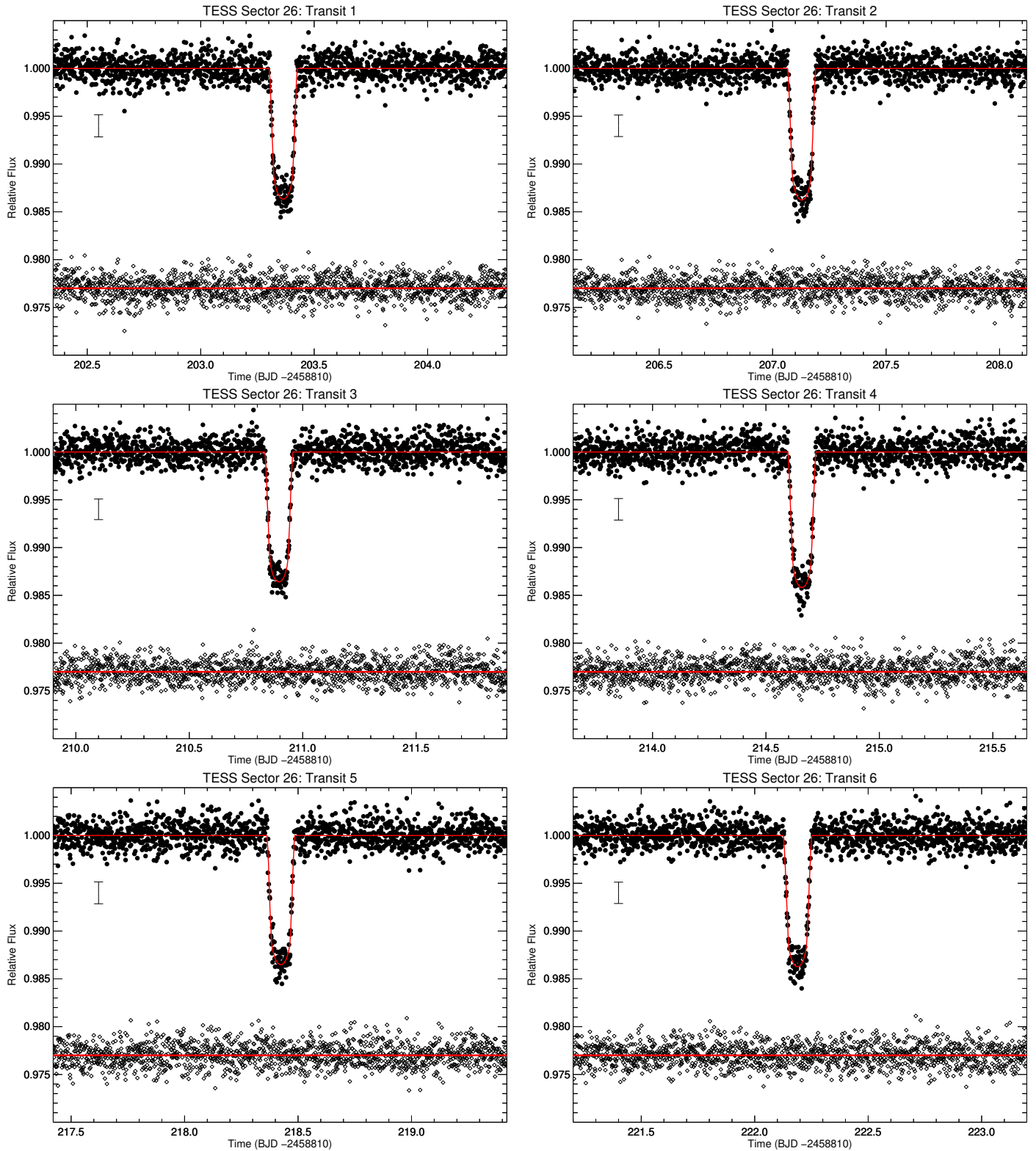


Figure 7. Individual TESS transit events from Sector 26 of XO-6b. The best-fitting model obtained from the EXOplanet MODELing Package (EXOMOP) is shown as a solid red line. The residuals (light curve - model) are shown below the light curve.

C. PARAMETERS DESCRIBING THE LIGHT-TIME EFFECT (LiTE) MODEL OF GARAI ET AL. (2020)

Table 3. Parameters describing the light-time effect (LiTE) model of Garai et al. (2020) that gave the best fit to their reported transit timing variations.

| Parameter | units | value |
|---------------|-----------|---------|
| P_{orb3} | days | 456 |
| $a \sin(i_3)$ | | 2.03 |
| e_3 | | 0.85 |
| $T(0)_3$ | BJD | 2458184 |
| ω_3 | $^\circ$ | 53 |
| K_3 | mins | 14.6 |
| $f(M_3)$ | M_\odot | 5.3 |

Where all parameters refer to the third body.

P_{orb3} is the orbital period,

a is the semi-major axis,

i_3 the inclination,

e_3 is the eccentricity,

$T(0)_3$ is the pericenter passage time,

ω_3 is the pericenter longitude,

K_3 is the semi-amplitude,

$f(M_3)$ is the mass function, $(a \sin(i_3))^3 / P_{orb3}^2$.

D. O-C VALUES FROM GARAI ET AL. (2020) AND BARYCENTRIC CORRECTIONS AT CORRESPONDING TRANSIT EPOCHS

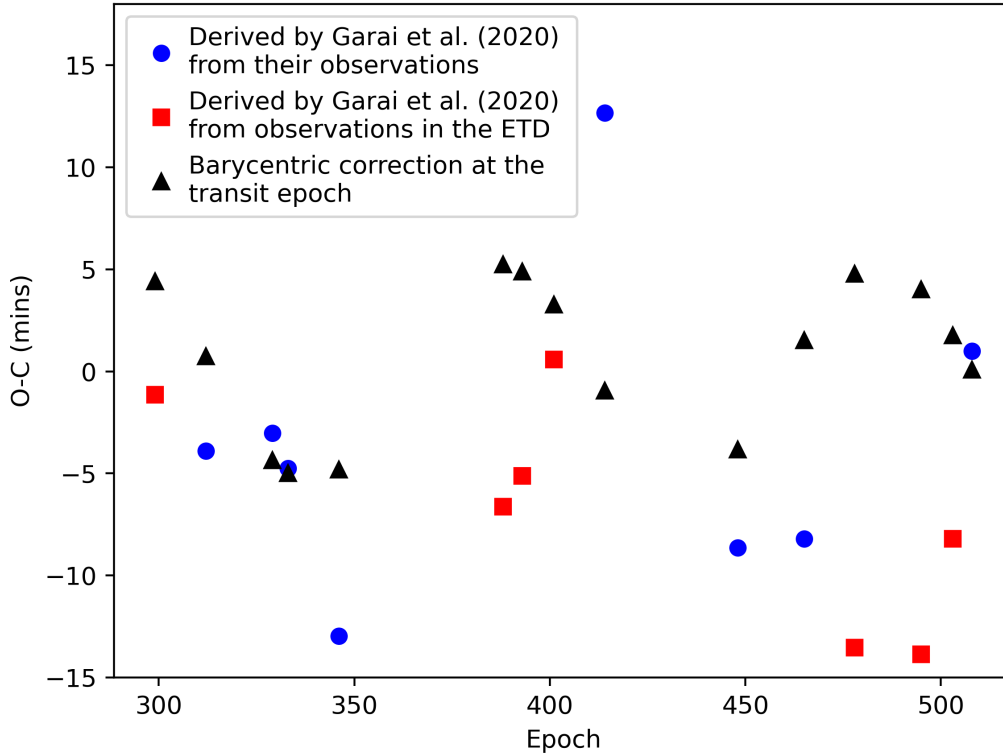


Figure 8. The TTVs reported by Garai et al. (2020) from their own observations (blue circles) and observations in the ETD (red squares). Additionally, the black triangles show the barycentric correction required at each transit epoch.

REFERENCES

- Astropy Collaboration, Robitaille, T. P., Tollerud, E. J., et al. 2013, *A&A*, 558, A33, doi: [10.1051/0004-6361/201322068](https://doi.org/10.1051/0004-6361/201322068)
- Baluev, R. V., Sokov, E. N., Jones, H. R. A., et al. 2019, *MNRAS*, 490, 1294, doi: [10.1093/mnras/stz2620](https://doi.org/10.1093/mnras/stz2620)
- Baluev, R. V., Sokov, E. N., Hoyer, S., et al. 2020, *MNRAS*, 496, L11, doi: [10.1093/mnrasl/slaa069](https://doi.org/10.1093/mnrasl/slaa069)
- Batygin, K., Bodenheimer, P. H., & Laughlin, G. P. 2016, *ApJ*, 829, 114, doi: [10.3847/0004-637X/829/2/114](https://doi.org/10.3847/0004-637X/829/2/114)
- Becker, J. C., Vanderburg, A., Adams, F. C., Rappaport, S. A., & Schwengeler, H. M. 2015, *ApJL*, 812, L18, doi: [10.1088/2041-8205/812/2/L18](https://doi.org/10.1088/2041-8205/812/2/L18)
- Bouma, L. G., Winn, J. N., Howard, A. W., et al. 2020, *ApJL*, 893, L29, doi: [10.3847/2041-8213/ab8563](https://doi.org/10.3847/2041-8213/ab8563)
- Bouma, L. G., Winn, J. N., Baxter, C., et al. 2019, *AJ*, 157, 217, doi: [10.3847/1538-3881/ab189f](https://doi.org/10.3847/1538-3881/ab189f)
- Braak, C. 2006, *Statistics and Computing*, 16, 239, doi: [10.1007/s11222-006-8769-1](https://doi.org/10.1007/s11222-006-8769-1)
- Carter, J. A., & Winn, J. N. 2009, *ApJ*, 704, 51, doi: [10.1088/0004-637X/704/1/51](https://doi.org/10.1088/0004-637X/704/1/51)
- Claret, A. 2017, *A&A*, 600, A30, doi: [10.1051/0004-6361/201629705](https://doi.org/10.1051/0004-6361/201629705)
- Cridland, A. J., van Dishoeck, E. F., Alessi, M., & Pudritz, R. E. 2019, *A&A*, 632, A63, doi: [10.1051/0004-6361/201936105](https://doi.org/10.1051/0004-6361/201936105)
- Crouzet, N., McCullough, P. R., Long, D., et al. 2017, *AJ*, 153, 94, doi: [10.3847/1538-3881/153/3/94](https://doi.org/10.3847/1538-3881/153/3/94)
- Dawson, R. I. 2020, *AJ*, 159, 223, doi: [10.3847/1538-3881/ab7fa5](https://doi.org/10.3847/1538-3881/ab7fa5)

- Dawson, R. I., Huang, C. X., Lissauer, J. J., et al. 2019, *AJ*, 158, 65, doi: [10.3847/1538-3881/ab24ba](https://doi.org/10.3847/1538-3881/ab24ba)
- Dragomir, D., Harris, M., Pepper, J., et al. 2020, *AJ*, 159, 219, doi: [10.3847/1538-3881/ab845d](https://doi.org/10.3847/1538-3881/ab845d)
- Eastman, J., Gaudi, B. S., & Agol, E. 2013, *PASP*, 125, 83, doi: [10.1086/669497](https://doi.org/10.1086/669497)
- Eastman, J., Siverd, R., & Gaudi, B. S. 2010, *PASP*, 122, 935, doi: [10.1086/655938](https://doi.org/10.1086/655938)
- Ford, E. B. 2006, *ApJ*, 642, 505, doi: [10.1086/500802](https://doi.org/10.1086/500802)
- Foreman-Mackey, D., Luger, R., Czekala, I., et al. 2020, *exoplanet-dev/exoplanet v0.3.2*, doi: [10.5281/zenodo.1998447](https://doi.org/10.5281/zenodo.1998447)
- Gajdoš, P., & Parimucha, Š. 2019, *Open European Journal on Variable Stars*, 197, 71
- Garai, Z., Pribulla, T., Komžík, R., et al. 2020, *MNRAS*, 491, 2760, doi: [10.1093/mnras/stz3235](https://doi.org/10.1093/mnras/stz3235)
- Gelman, A., & Rubin, D. B. 1992, *Statist.Sci.*, 7, 457
- Hadden, S., Barclay, T., Payne, M. J., & Holman, M. J. 2019, *AJ*, 158, 146, doi: [10.3847/1538-3881/ab384c](https://doi.org/10.3847/1538-3881/ab384c)
- Herman, M. K., de Mooij, E. J. W., Huang, C. X., & Jayawardhana, R. 2018, *AJ*, 155, 13, doi: [10.3847/1538-3881/aa991f](https://doi.org/10.3847/1538-3881/aa991f)
- Hrudková, M., Skillen, I., Benn, C. R., et al. 2010, *MNRAS*, 403, 2111, doi: [10.1111/j.1365-2966.2010.16247.x](https://doi.org/10.1111/j.1365-2966.2010.16247.x)
- Huang, C., Wu, Y., & Triaud, A. H. M. J. 2016, *ApJ*, 825, 98, doi: [10.3847/0004-637X/825/2/98](https://doi.org/10.3847/0004-637X/825/2/98)
- Jenkins, J. M., Twicken, J. D., McCauliff, S., et al. 2016, in *Society of Photo-Optical Instrumentation Engineers (SPIE) Conference Series*, Vol. 9913, *Software and Cyberinfrastructure for Astronomy IV*, 99133E, doi: [10.1117/12.2233418](https://doi.org/10.1117/12.2233418)
- Luger, R., Agol, E., Kruse, E., et al. 2016, *AJ*, 152, 100, doi: [10.3847/0004-6256/152/4/100](https://doi.org/10.3847/0004-6256/152/4/100)
- Maciejewski, G., Dimitrov, D., Fernández, M., et al. 2016, *A&A*, 588, L6, doi: [10.1051/0004-6361/201628312](https://doi.org/10.1051/0004-6361/201628312)
- Maciejewski, G., Fernández, M., Aceituno, F., et al. 2018, *AcA*, 68, 371, doi: [10.32023/0001-5237/68.4.4](https://doi.org/10.32023/0001-5237/68.4.4)
- Mandel, K., & Agol, E. 2002, *ApJL*, 580, L171, doi: [10.1086/345520](https://doi.org/10.1086/345520)
- Masuda, K. 2015, *ApJ*, 805, 28, doi: [10.1088/0004-637X/805/1/28](https://doi.org/10.1088/0004-637X/805/1/28)
- Mazeh, T., Nachmani, G., Holzer, T., et al. 2013, *ApJS*, 208, 16, doi: [10.1088/0067-0049/208/2/16](https://doi.org/10.1088/0067-0049/208/2/16)
- Mustill, A. J., Davies, M. B., & Johansen, A. 2015, *ApJ*, 808, 14, doi: [10.1088/0004-637X/808/1/14](https://doi.org/10.1088/0004-637X/808/1/14)
- Nesvorný, D. 2009, *ApJ*, 701, 1116, doi: [10.1088/0004-637X/701/2/1116](https://doi.org/10.1088/0004-637X/701/2/1116)
- Öberg, K. I., Murray-Clay, R., & Bergin, E. A. 2011, *ApJL*, 743, L16, doi: [10.1088/2041-8205/743/1/L16](https://doi.org/10.1088/2041-8205/743/1/L16)
- Patra, K. C., Winn, J. N., Holman, M. J., et al. 2017, *AJ*, 154, 4, doi: [10.3847/1538-3881/aa6d75](https://doi.org/10.3847/1538-3881/aa6d75)
- Pearson, K. A. 2019, *AJ*, 158, 243, doi: [10.3847/1538-3881/ab4e1c](https://doi.org/10.3847/1538-3881/ab4e1c)
- Pearson, K. A., Turner, J. D., & Sagan, T. G. 2014, *NewA*, 27, 102, doi: [10.1016/j.newast.2013.08.002](https://doi.org/10.1016/j.newast.2013.08.002)
- Poddany, S., Brát, L., & Pejcha, O. 2010, *NewA*, 15, 297, doi: [10.1016/j.newast.2009.09.001](https://doi.org/10.1016/j.newast.2009.09.001)
- Pont, F., Zucker, S., & Queloz, D. 2006, *MNRAS*, 373, 231, doi: [10.1111/j.1365-2966.2006.11012.x](https://doi.org/10.1111/j.1365-2966.2006.11012.x)
- Ricker, G. R., Winn, J. N., Vanderspek, R., et al. 2014, in *Society of Photo-Optical Instrumentation Engineers (SPIE) Conference Series*, Vol. 9143, *Proc. SPIE*, 914320, doi: [10.1117/12.2063489](https://doi.org/10.1117/12.2063489)
- Safronov, V. S. 1972, *Evolution of the protoplanetary cloud and formation of the earth and planets*. (Keter Publishing House)
- Seager, S., & Mallén-Ornelas, G. 2003, *ApJ*, 585, 1038, doi: [10.1086/346105](https://doi.org/10.1086/346105)
- Southworth, J. 2008, *MNRAS*, 386, 1644, doi: [10.1111/j.1365-2966.2008.13145.x](https://doi.org/10.1111/j.1365-2966.2008.13145.x)
- . 2010, *MNRAS*, 408, 1689, doi: [10.1111/j.1365-2966.2010.17231.x](https://doi.org/10.1111/j.1365-2966.2010.17231.x)
- Southworth, J., Wheatley, P. J., & Sams, G. 2007, *MNRAS*, 379, L11, doi: [10.1111/j.1745-3933.2007.00324.x](https://doi.org/10.1111/j.1745-3933.2007.00324.x)
- Southworth, J., Dominik, M., Jørgensen, U. G., et al. 2019, *MNRAS*, 490, 4230, doi: [10.1093/mnras/stz2602](https://doi.org/10.1093/mnras/stz2602)
- Spalding, C., & Batygin, K. 2016, *ApJ*, 830, 5, doi: [10.3847/0004-637X/830/1/5](https://doi.org/10.3847/0004-637X/830/1/5)
- Steffen, J. H., Ragozzine, D., Fabrycky, D. C., et al. 2012, *Proceedings of the National Academy of Science*, 109, 7982, doi: [10.1073/pnas.1120970109](https://doi.org/10.1073/pnas.1120970109)
- Szabó, G. M., Pribulla, T., Pál, A., et al. 2020, *MNRAS*, 492, L17, doi: [10.1093/mnras/slz177](https://doi.org/10.1093/mnras/slz177)
- Szabó, G. M., Simon, A., & Kiss, L. L. 2014, *MNRAS*, 437, 1045, doi: [10.1093/mnras/stt1724](https://doi.org/10.1093/mnras/stt1724)
- Turner, J. D., Pearson, K. A., Biddle, L. I., et al. 2016, *MNRAS*, 459, 789, doi: [10.1093/mnras/stw574](https://doi.org/10.1093/mnras/stw574)
- Turner, J. D., Leiter, R. M., Biddle, L. I., et al. 2017, *MNRAS*, 472, 3871, doi: [10.1093/mnras/stx2221](https://doi.org/10.1093/mnras/stx2221)
- von Essen, C., Lund, M. N., Handberg, R., et al. 2020, *AJ*, 160, 34, doi: [10.3847/1538-3881/ab93dd](https://doi.org/10.3847/1538-3881/ab93dd)
- Winn, J. N. 2010, preprint (arXiv:1001.2010). <https://arxiv.org/abs/1001.2010>
- Yee, S. W., Winn, J. N., Knutson, H. A., et al. 2020, *ApJL*, 888, L5, doi: [10.3847/2041-8213/ab5c16](https://doi.org/10.3847/2041-8213/ab5c16)
- Zellem, R. T., Pearson, K. A., Blaser, E., et al. 2020, *PASP*, 132, 054401, doi: [10.1088/1538-3873/ab7ee7](https://doi.org/10.1088/1538-3873/ab7ee7)